Human Molecular Genetics, 2016, Vol. 25, No. 21 4635–4648

doi: 10.1093/hmg/ddw292
Advance Access Publication Date: 29 August 2016
Original Article

ORIGINAL ARTICLE

Infantile neurodegenerative disorder associated with mutations in *TBCD*, an essential gene in the tubulin heterodimer assembly pathway

Shimon Edvardson[1,5,†,*], Guoling Tian[2,†], Hayley Cullen[3,†], Hannah Vanyai[3], Linh Ngo[3], Saiuj Bhat[3], Adi Aran[4], Muhannad Daana[5], Naderah Da'amseh[6], Bassam Abu-Libdeh[6], Nicholas J. Cowan[2,#], Julian Ik-Tsen Heng[3,#] and Orly Elpeleg[1,#]

[1]Monique and Jacques Roboh Department of Genetic Research, Hadassah, Hebrew University Medical Center Jerusalem, Jerusalem, Israel, [2]Department of Biochemistry & Molecular Pharmacology, NYU Langone Medical Center, New York, NY, USA, [3]The Harry Perkins Institute of Medical Research, QEII Medical Centre and Centre for Medical Research, the University of Western Australia, Nedlands, Western Australia, Australia, [4]Neuropediatric Unit, Shaare Zedek Medical Center; Hebrew University-Hadassah School of Medicine, Jerusalem, Israel, [5]Neuropediatric Unit, Hadassah Hebrew University Medical Center, Jerusalem, Israel and [6]Department of Pediatrics and Genetics, Makassed Hospital, Al-Quds Medical School, Jerusalem

*To whom correspondence should be addressed at: Shimon Edvardson, Pediatric Neurology Unit, Hadassah University Hospital, Mount Scopus, Jerusalem, Israel. Email: simon@hadassah.org.il

Abstract

Mutation in a growing spectrum of genes is known to either cause or contribute to primary or secondary microcephaly. In primary microcephaly the genetic determinants frequently involve mutations that contribute to or modulate the microtubule cytoskeleton by causing perturbations of neuronal proliferation and migration. Here we describe four patients from two unrelated families each with an infantile neurodegenerative disorder characterized by loss of developmental milestones at 9–24 months of age followed by seizures, dystonia and acquired microcephaly. The patients harboured homozygous missense mutations (A475T and A586V) in *TBCD*, a gene encoding one of five tubulin-specific chaperones (termed TBCA-E) that function in concert as a nanomachine required for the de novo assembly of the α/β tubulin heterodimer. The latter is the subunit from which microtubule polymers are assembled. We found a reduced intracellular abundance of TBCD in patient fibroblasts to about 10% (in the case of A475T) or 40% (in the case of A586V) compared to age-matched wild type controls. Functional analyses of the mutant proteins revealed a partially compromised ability to participate in the heterodimer

[†]These authors contributed equally to this work.
[#]Equal senior contributing authors.

Julian Heng, The Harry Perkins Institute of Medical Research, QEII Medical Centre and Centre for Medical Research, the University of Western Australia, Nedlands 6009, Western Australia, Australia. Email:julian.heng@perkins.uwa.edu.au.
Nicholas J. Cowan, Department of Biochemistry & Molecular Pharmacology, NYU Langone Medical Center, New York NY 10016, USA. Email:nicholas.cowan@nyumc.org.
Orly Elpeleg, Monique and Jacques Roboh Department of Genetic Research, Hadassah, Hebrew University Medical Center Jerusalem, Jerusalem, Israel. Email:elpeleg@hadassah.org.il.

Received: June 2, 2016. **Revised:** August 5, 2016. **Accepted:** August 25, 2016

assembly pathway. We show via *in utero* shRNA-mediated suppression that a balanced supply of tbcd is critical for cortical cell proliferation and radial migration in the developing mouse brain. We conclude that *TBCD* is a novel functional contributor to the mammalian cerebral cortex development, and that the pathological mechanism resulting from the mutations we describe is likely to involve compromised interactions with one or more TBCD-interacting effectors that influence the dynamics and behaviour of the neuronal cytoskeleton.

Introduction

Microcephaly is a condition in which the head circumference is more than 3 SD below the normal value for a given age, and is typically associated with intellectual disability as a consequence of impaired brain growth. Primary microcephaly is present at birth, and has been associated with autosomal recessive mutations in a spectrum of genes that contribute to the normal proliferation of neural progenitors during cortical development (1). Secondary microcephaly is distinguished from primary microcephaly in that it refers to postnatal slowing or arrest of head circumference growth, and may be due to slowed growth of the brain or atrophy of either the white or gray matter. Prenatal brain growth is attributed to neuronal proliferation and migration, and is thus sensitive to perturbations of the microtubule machinery essential to the organization of the mitotic spindle and microtubule polymers. In contrast, postnatal growth largely reflects glial proliferation and the deposition of myelin (2). Atrophy or arrested growth of the infantile brain may be caused by a multitude of exogenous or genetic/metabolic causes (3), but this is rarely attributed to microtubule dysfunction. Many of the genes known to contribute to microcephaly influence centrosome function, thus highlighting the important role that these complex and independently replicating organelles play in the regulation of cell division by organizing the activity of dynamic mitotic spindle microtubules. The critical contribution of properly regulated microtubule-based events to brain development has been further underscored by the discovery of a range of devastating brain disorders - collectively known as the tubulinopathies - caused by mutation in one of the genes encoding α- or β-tubulin (4–11), the tightly associated components of the heterodimer that assembles to form microtubule polymers.

It has never proven possible to obtain α- or β-tubulin free from its cognate partner. This fact is explained by the discovery that a multi-component molecular machine is required to assemble the tubulin heterodimer (12). The assembly process involves several steps. Newly synthesized α- and β-tubulin polypeptides are stabilized by interaction with prefoldin (13), a hetero-hexameric chaperone that binds and transfers tubulin target proteins to the cytosolic chaperonin, CCT. As a result of multiple rounds of ATP-dependent binding to and discharge from the chaperonin's interactive surfaces (14), α- and β-tubulins assume a quasi-native conformation (15). Thereafter, these intermediates interact with a series of five tubulin-specific chaperones (termed TBCA-E); these function together as a nanomachine that assembles the α/β tubulin heterodimer (12,16) (Supplementary Material, Fig. S1). Here we describe four patients from two families with secondary microcephaly harbouring homozygous mutations in *TBCD*. We present a comprehensive biochemical and cell biological analysis of the effect of these mutations on the ability of the mutant proteins to participate in the tubulin heterodimer assembly and disassembly pathways, and on the effect of perturbing TBCD levels in the developing mammalian brain. Our data point to disruption of a balanced level of TBCD as well as compromised interaction with TBCD effectors as contributing factors to the pathogenesis of the neurodegenerative diseases we describe.

Results

Patients

The patients were four girls, the only offspring of two consanguineous couples, originating from the Cochin-Jewish community which resides in southwestern India (family A) and from a Moslem-Palestinian community (family B) (Fig. 1A and B). At the time of reporting, patient AII-1 and patient AII-2 were 5 and 2 years old, respectively. Both presented with severe global developmental delay, dystonia, intractable seizures and brain atrophy. They were born after uneventful pregnancies and their perinatal course was normal. Both were diagnosed with bilateral developmental dislocation of the hips soon after birth and were treated with casts and braces. Patient AII-1 required pelvic osteotomy at 30 months due to residual dysplasia. Initial concern regarding development was raised at 3–5 months of age due to the absence of motor milestones, although the delay was attributed to the casts and braces. Patient AII-1 reached peak development at 10 months when she could sit without support, clap hands, laugh socially and mumble. Despite adequate habilitation, these milestones were lost and at present she can hardly make eye contact and can no longer sit or perform voluntary motor acts. Epilepsy, acquired borderline microcephaly (current head circumference 46 cm, $P = 3\%$, while at birth 34.7 cm, $P = 50\%$) and severe dystonia all emerged during the first year of life. Seizures were initially triggered by fever and consisted mainly of tonic posturing for 2–3 minutes, but later these were non-triggered. Her physical examination is notable for dystonia, hirsutism, strabismus and vertical nystagmus. Deep tendon reflexes are brisk but without clonus or positive Babinsky's sign. Brain MRI at age 13 months (Fig. 2A) disclosed generalized brain atrophy, mainly of white matter but also prominent in the cortex and cerebellum. ABR has been repeatedly normal, but visual evoked potentials demonstrated bilateral prolonged response times at 18 months of age. Patient AII-2 has followed a similar course. At the peak of her development at 14 months of age, she could utter syllables, sit and reach for objects, but with dystonic movements and motor apraxia. Her vision and hearing tests are normal. Tonic seizures during fever (similar to those in her sister) started at 8 months and are well controlled with Levetiracetam. Acquired microcephaly (H.C. 42cm, <3%), hirsutism, strabismus, nystagmus, severe dystonia, brisk DTRs and motor apraxia were noted on latest follow-up. Brain MRI at the age of 8 months (Fig. 2B) revealed brain atrophy with a paucity of white matter, a thin corpus callosum and cerebellar atrophy.

Both affected children in family B had normal pregnancies and perinatal course followed age-appropriate achievement of milestones up to 1 year of age when peak expressive language development consisted of a few words and walking had been achieved. Subsequent development was absent, and from age 2 to 3 years

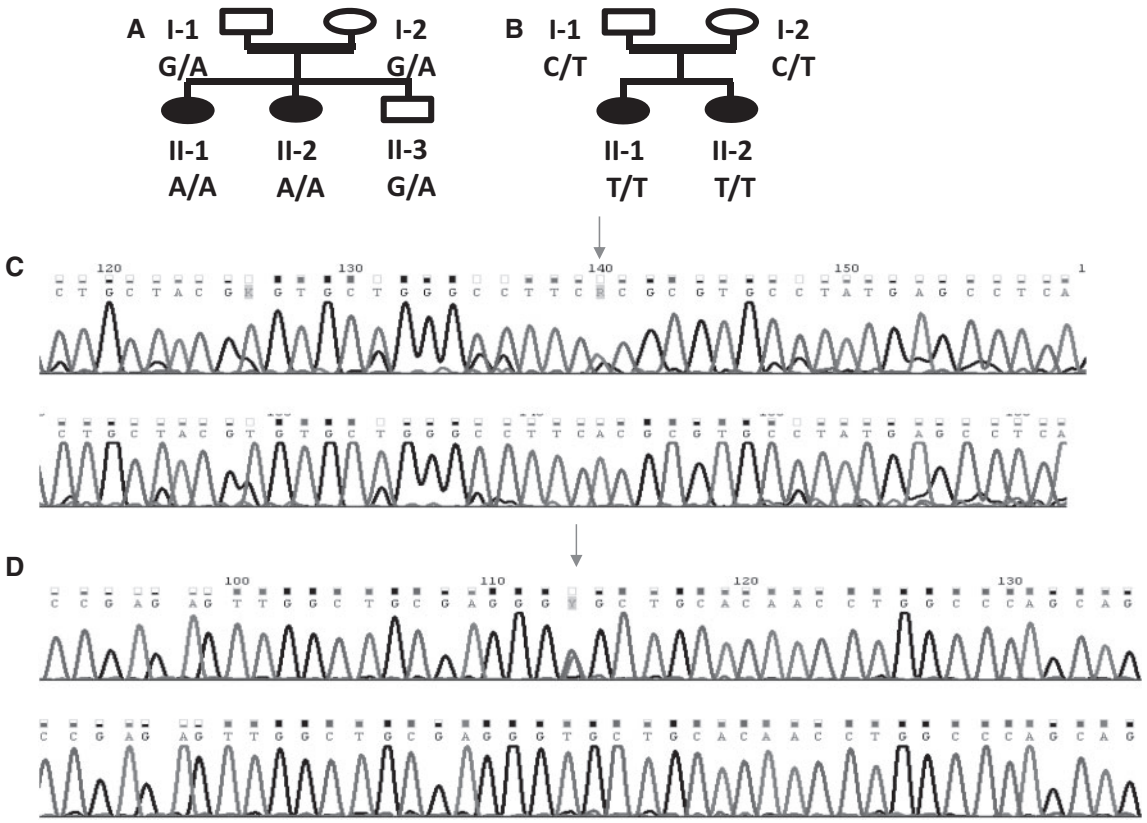

Figure 1. Patient pedigrees and identification of mutations in *TBCD*. **(A, B)** Pedigrees of families A and B (see text). **(C, D)** DNA sequence traces showing mutations (arrowed) in *TBCD* in patients AII-1, AII-2 **(C)** and BII-1 and BII-2 **(D)**, respectively, together with corresponding heterozygous controls.

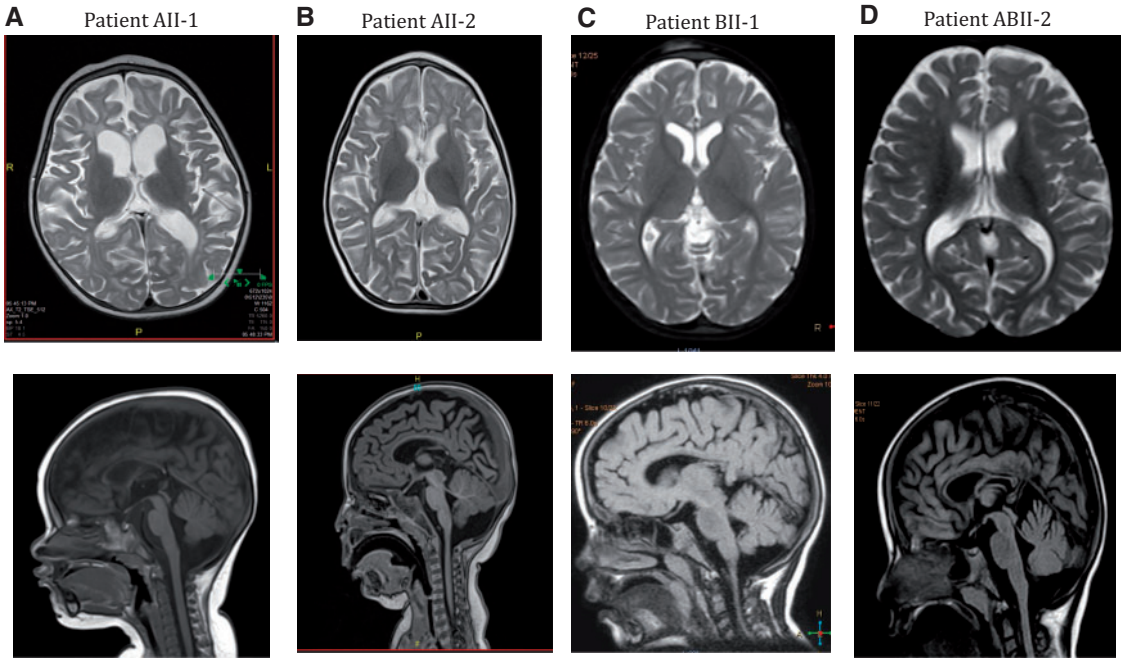

Figure 2. MRI of patient brains **(A)** Patient AII-1 at 13 months. **(B)** Patient AII-2 at age 8 months. **(C)** Patient BII-1 at age 4 years. **(D)** Patient BII-2 at age 4 years. Top panels showing Axial T2-weighted images. Bottom images showing Midsagittal T1-weighted images. Note brain atrophy and paucity of white matter, as well as a thin corpus callosum and cerebellar atrophy visible in bottom images.

Table 1. Summary of patient clinical features

Patient	Current Age/sex	Arrest of development	Epilepsy	Dystonia	Nystagmus	Spasticity	Brain MRI
AII-1	5Y./F	10 months	Severe, Initially with fever	Y	Y	N	Generalized atrophy, mainly white matter
AII-2	2 Y./F	14 months	Infrequent, Initially with fever	Y	Y	N	Generalized atrophy, mainly of white matter, thin CC
B-1	6.3 Y./F	12 months	Rare	Y	N	Y	Generalized atrophy, mainly of white matter, thin CC
B-2	4 Y./F	12 months	Rare	Y	N	Y	Generalized atrophy, mainly of white matter, thin CC

CC = corpus callosum.

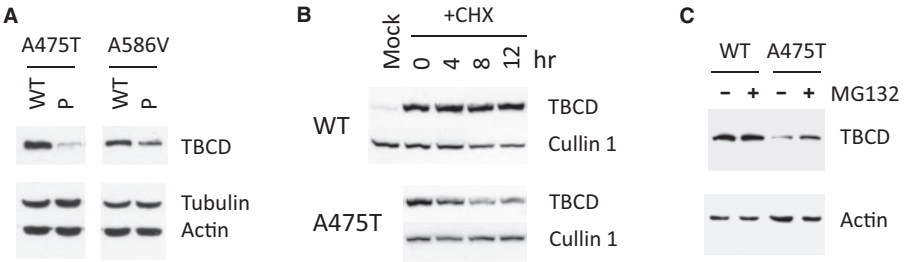

Figure 3. TBCD and tubulin abundance in patient skin fibroblasts and foreshortened half life of A475T TBCD as a result of targeted proteasomal degradation (**A**) Aliquots of supernatants containing 10 μg of total protein prepared from wild type or patient fibroblasts were assayed by Western blotting using antibodies specific for human TBCD (21) (top), a monoclonal anti-α-tubulin antibody (middle) and an anti-actin monoclonal antibody (used as a loading control) (bottom). Note the dramatic reduction (compared to wild type) in the abundance of TBCD in A475T (and to a lesser extent A586V) patient cells, with no significant change in the level of tubulin compared to control cells in either case. (**B**) Hela cells were transfected with constructs engineered for the expression of either wild type or mutant (A475T) TBCD. After 42 h, cycloheximide (CHX) was added to the culture medium; at the times (in h) indicated in the Figure, a soluble extract was prepared and the TBCD content in aliquots containing equal amounts of total protein measured by Western blotting using an anti-human TBCD-specific antibody (21). A mock-transfected control is included at the left; a Cullin-1 specific antibody was used in parallel as a loading control. Note the conspicuous decay in the abundance of TBCD in cells transfected with TBCD A475T compared to the (stable) wild type control. (**C**) Whole cell extracts of wild type or A475T patient-derived fibroblasts incubated for 12 h either in the absence (-) or presence (+) of the proteasome inhibitor MG132 were analysed by Western blotting with an anti-human TBCD antibody; an anti-β-actin antibody was used as a loading control. Note the enhanced level of TBCD present in A475T-derived cells as a consequence of incubation with MG132.

loss of previous milestones occurred. Currently at age 6.3 years and 48 months, both lack purposeful movement and language. Both have suffered rare seizures and are spastic, dystonic and microcephalic (48.2 and 46.2 cm, respectively, both < 3%). Brain MRI at age 4 years revealed an abnormal paucity of white matter with a thin corpus callosum and cerebellar atrophy (Fig. 2C and D). A summary of the patients' clinical features is presented in Table 1.

Exome analysis

Exome analyses of DNA from patients AII-1 and BII-1 yielded 49.71 and 47.10 million confidently mapped reads with an average coverage of X55 and X57, respectively. Following alignment to the reference genome (Hg19) and variant calling, we removed variants which were called less than X8, were off-target, heterozygous, synonymous, MAF > 0.1% in dbSNP140 or present at >1% in the Hadassah in-house database. Five and seven variants remained in the respective samples (Supplementary Material, Table S1), but only one segregated with the disease in each family and affected a gene of neurological relevance. For the patients in family A, this was Chr17: 80828204 G > A, NM_005993 c.G1423A, p.A475T in the gene encoding TBCD, and for family B, it was Chr17: 80861307 C > T, NM_005993 c.C1757T, p.A586V in the gene encoding TBCD (Fig. 1C and D). Both mutations affected highly conserved residues and both were extremely rare among healthy individuals; among the ~60,000 exome analysis deposited in ExAC version 0.3 (Exome Aggregation Consortium, Cambridge, MA, (URL: http://exac.broadinstitute.org)), only two individuals carried the p.A475T mutation and none carried the p.A586V mutation.

Diminished TBCD abundance in patient fibroblasts

We examined patient-derived cultured skin fibroblasts by immunofluorescence using an anti α-tubulin antibody (5) and by Western blotting of whole cell extracts. We found no detectable abnormalities in either the density or organization of cellular microtubules or in the overall level of tubulin in either A475T or A586V fibroblasts compared to age-matched controls (Supplementary Material, Fig. S2). Nor did we observe any difference in growth rate (doubling time) or the number of mitotic figures between wild type and patient-derived fibroblast cultures (data not shown). Strikingly, however, Western blotting of cytosolic extracts reproducibly revealed a dramatic reduction in the abundance of TBCD in A475T patient-derived cells to about 10% compared to an age-matched wild type control, and a more modest corresponding reduction (to about 40%) in A586V patient-derived cells (Fig. 3A).

Compromised TBCD stability and activity in heterodimer assembly/disassembly

We investigated the mechanism leading to the diminished levels of TBCD present in patient-derived cells. We first examined

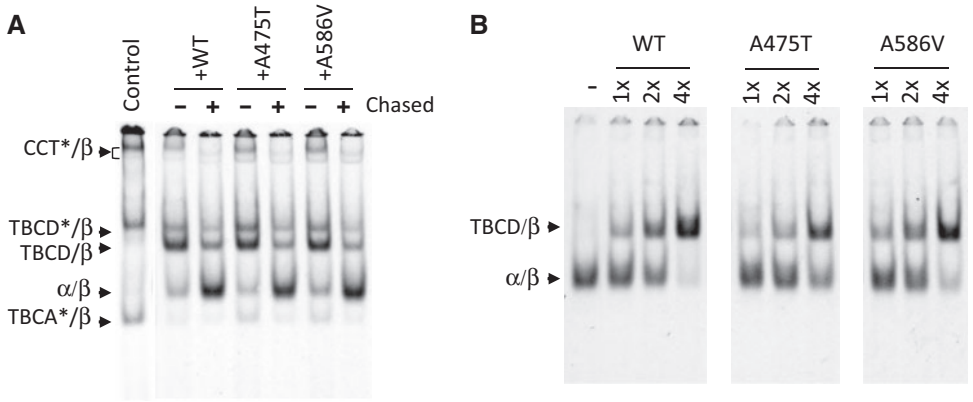

Figure 4. Effect of TBCD mutations on tubulin heterodimer assembly *in vitro* **(A)** Forward tubulin folding reactions in which coupled transcription/translation reactions done in rabbit reticulocyte lysate supplemented with ^{35}S-methionine were driven by a plasmid encoding full-length mouse *tubb3* β-tubulin (17) by incubation at 30°C up to a point (t = 40 min) immediately before significant accumulation of the TBCD/β-tubulin intermediate occurs (10) and then supplemented with human recombinant TBCD (see Methods). All reaction products were analysed by resolution on 4.5% native polyacrylamide gels (10) followed by autoradiography. Lanes marked – and + show reaction products formed either without (-) or with (+) the chase with added tubulin heterodimers. Arrows (top to bottom) show the migration positions of the (rabbit) CCT/β-tubulin binary complex, the rabbit and human TBCD/β-tubulin co-complexes, native tubulin heterodimers, and the (rabbit) TBCA/β-tubulin co-complex, respectively. Products of rabbit origin generated via interaction of β-tubulin polypeptides with TBCs intrinsic to the reticulocyte lysate cocktail are marked with an asterisk. **(B)** Heterodimer disruption reactions in which purified tubulin heterodimers ^{35}S-labelled in their β-subunits were incubated at the stoichiometric ratios shown in the Figure with respect to recombinant wild type or mutant TBCD (Supplementary Material, Fig. 4). Reaction products were analysed as in (B). Arrows (upper and lower) show the migration positions of the TBCD/β-tubulin complex and native tubulin heterodimers, respectively. Note the reduced extent to which recombinant TBCD A475T (and to a lesser extent TBCD A586V) are capable of disrupting native ^{35}S-labelled heterodimers compared to the wild type control.

translational inefficiency, misfolding or structural instability of mutant TBCDs as potential causes of reduced intracellular TBCD abundance, and found no significant differences compared to a wild type control (Supplementary Material, Fig. S3A–C). On the other hand, when wild type and mutant proteins were expressed via transfection in cultured cells, the A475T mutant protein had a significantly foreshortened half-life compared to the wild type control (Fig. 3B). We also incubated wild type and A475T-derived primary skin fibroblasts for 12 h with the potent proteasomal inhibitor MG132, and compared their TBCD content by Western blotting. This experiment showed a significant elevation in the level of TBCD in A475T cells, but not in the wild type control (Fig. 3C). We conclude that the reduced level of TBCD present in A475T (and presumably also A586V) patient cells is a consequence of a change in TBCD secondary or tertiary structure such that the mutant proteins are vulnerable to targeted destruction via the ubiquitin proteasome degradation pathway.

We next determined the ability of the mutant TBCDs to function in *in vitro* heterodimer assembly reactions (see Supplementary Material, Fig. S1). In these experiments, we used a cloned cDNA encoding a full-length β-tubulin (17) to drive expression in a rabbit reticulocyte lysate cell-free system supplemented with ^{35}S-methionine. The reactions were allowed to proceed until a point (at t = 40 min) where there is only a modest accumulation of the TBCD/β-tubulin intermediate (10) (Fig. 4A, left hand track). With the exception of this control reaction (done to reveal the migration position of endogenous reaction products of rabbit origin), a large stoichiometric excess of recombinant human TBCD (wild type [+WT] or mutant [+A475T, +A586V]; Supplementary Material, Fig. S4) was added to the TNT cocktail and the incubation continued for a further 30 min. The reaction products were divided equally; one aliquot was supplemented with native tubulin heterodimers (18) so as to chase the TBCD/β-tubulin intermediates into de novo assembled heterodimers, and both aliquots were then incubated for a further 30 min (Fig. 4A, tracks marked – or +). This experiment – in which the full spectrum of (rabbit) chaperones required to generate de novo assembled heterodimers is provided by the lysate (12) – showed that both wild type and mutant human TBCDs can compete successfully for rabbit CCT-generated β-tubulin folding intermediates, and that these TBCD-bound intermediates can be discharged into native heterodimers. We conclude that the A475T and A586V mutant TBCDs are functionally capable of participating in the heterodimer assembly reaction.

To assess this functionality in a quantitative manner, we tested the ability of recombinant wild type and mutant TBCDs to participate in biochemically defined *in vitro* back-reactions (see Supplementary Material, Fig. S1). In these experiments, we prepared purified tubulin heterodimers ^{35}S-labelled in their β-tubulin subunits (19) and incubated them in the presence of an increasing stoichiometric abundance of either recombinant wild type or mutant forms of TBCD. The ability of the various forms of TBCD to disrupt the labelled heterodimers was then assessed following analysis of the reaction products on a non-denaturing gel. This experiment showed that TBCD A475T, and to a lesser extent A586V, had a diminished capacity to disrupt tubulin heterodimers compared to the wild type protein (Fig. 4B): in the presence of a 4-fold stoichiometric excess of TBCD, almost all tubulin heterodimers were disrupted to form the TBCD/β-tubulin intermediate in the case of the wild type protein, whereas in the case of TBCD A475T and A586V (particularly the former), the disruption reactions were significantly less efficient. Because TBCD-mediated tubulin disruption is simply the heterodimer assembly reaction in reverse, we conclude that both mutant TBCDs (A475T to a greater extent than A586V) are less efficient than wild type TBCD in their ability to contribute to the generation of de novo assembled heterodimers.

Activity of mutant TBCDs *in vivo*

We extended these *in vitro* observations by measuring the ability of mutant TBCDs to participate in the back-reaction *in vivo*. In this scenario, expression of an overabundance of human TBCD results in varying degrees of microtubule

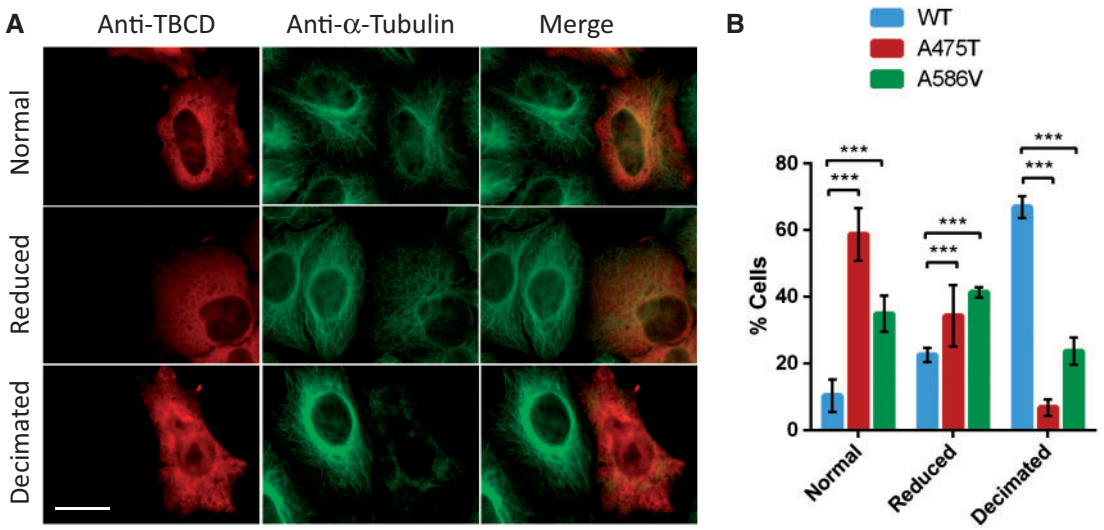

Figure 5. Effect of wild type and mutant TBCD expression on microtubule architecture in Arl2-suppressed HeLa cells (**A**) Immunofluorescence analyses showing varying degrees of disruption of normal microtubule architecture (reduced density) or destruction (obliteration) in HeLa cells overexpressing wild type TBCD following siRNA-induced suppression of Arl2 expression. Panels show examples of cells expressing TBCD (shown in red) with microtubule phenotypes (shown in green) classified as follows: Top row: normal; Centre row: reduced microtubule abundance; Lower row: microtubule obliteration. Scale bar = 20μ. **(B)** Quantification of phenotypes (defined in (A)) in HeLa cells overexpressing wild type (left), A475T (centre) and A586V (right) TBCD. There was a significant interaction between expressed TBCD variant (wild type or mutant) and microtubule phenotype (i.e. normal, reduced, decimated) ($F_{4,18} = 93$, $P < 0.0001$, $n = 3$ per condition). Scale bars represent mean ± SD.

depolymerization as a result of tubulin heterodimer disruption in cells in which expression of the TBCD regulator Arl2 (20) has been suppressed (21). We classified the microtubule phenotype in TBCD overexpressing cells into three groups defined by the extent of microtubule depletion. In the case of wild type TBCD, we found that more than half of the transfected cells had lost the vast majority of their microtubules ("decimated", Fig. 5A; quantitatively analysed in Fig. 5B). In contrast, in cells overexpressing mutant TBCDs, there were many fewer cells displaying a microtubule decimation phenotype, particularly in the case of the A475T mutation, and an increase in the relative number of cells displaying either an unimpaired microtubule cytoskeleton or only moderate microtubule depletion ("normal" and "reduced", respectively: Fig. 5A, B). These *in vivo* data reinforce our conclusion based on *in vitro* analyses that both mutant TBCDs are compromised in their ability to efficiently participate in tubulin heterodimer assembly/disassembly reactions.

Disruptions to TBCD expression in the developing mammalian cerebral cortex

Measurement of TBCD steady state protein levels in brain extracts from embryonic and early post-natal mice showed maximal expression at E14.5, consistent with a requirement for TBCD during a peak in cortical neurogenesis (22,23), together with a second small burst of expression at postnatal day 5 (P5) (Fig. 6A). To address the role of TBCD at the physiological level, we performed functional experiments to manipulate TBCD expression in the developing mouse brain. We designed several shRNA targeting vectors contained in plasmids encoding a bright GFP cassette, and selected two of these for their potential ability to suppress expression of endogenous tbcd in Neuro2A cells. The result of this experiment showed that shRNA3 (denoted sh3) had the strongest capacity to reduce steady state levels of TBCD (Supplementary Material, Fig. S5). We then performed *in utero* electroporation to introduce the sh3 vector into the cortical cells which line the ventricular germinal zone of the embryonic day (E)14.5 forebrain, and examined the treated cells two days later (i.e. at E16.5). DNA electroporations for each treatment condition were performed using a balanced stoichiometry of shRNA vector and mammalian expression vector (i.e. containing either encoded TBCD or lacking any encoded sequence, as appropriate). A previously characterized, non-targeting shRNA control vector (denoted "Control") (24) was used alongside *tbcd* shRNA experiments. Compared to *in utero* electroporation of the control (non-targeting) shRNA, co-electroporation of a plasmid engineered for the expression of wild type TBCD resulted in a significant reduction in GFP-labelled cells that co-labelled with the mitotic marker pH3 (Fig. 6B,C and F). Similarly, suppression of endogenous tbcd by shRNA3 also led to a significant reduction in the number of cells expressing pH3 (Fig. 6D and F). We corroborated these findings via parallel electroporation experiments using an additional targeting shRNA; treatment with shRNA2 also led to a reduction in pH3 levels (Supplementary Material, Fig. S6A–D). We also studied the position of pH3-labelled mitotic indices that are indicative of a surface division (i.e. pH3+ mitoses lying immediately adjacent to the lateral ventricle, highlighted with arrowheads in Fig. 6F) as well as non-surface division (i.e. pH3+ mitoses away from the ventricular wall, highlighted with arrows in Fig. 6F) in our experiments. We found that forced expression of TBCD or knockdown with shRNAs led to a significant reduction in both surface and non-surface divisions (Fig. 6G and H). However, co-delivery of wild type TBCD can restore pH3 expression in sh3-treated cells to levels that are not significantly different to the control (Fig. 6E, $F_{3,15} = 13.17$, $P = 0.0002$ one-way ANOVA, $n = 4$–6 samples per condition). In addition, we performed immunostaining with activated Caspase 3 (a marker of programmed cell death) and found no significant difference between treatment groups, ruling out this potential confound for our observations (Supplementary Material, Fig.

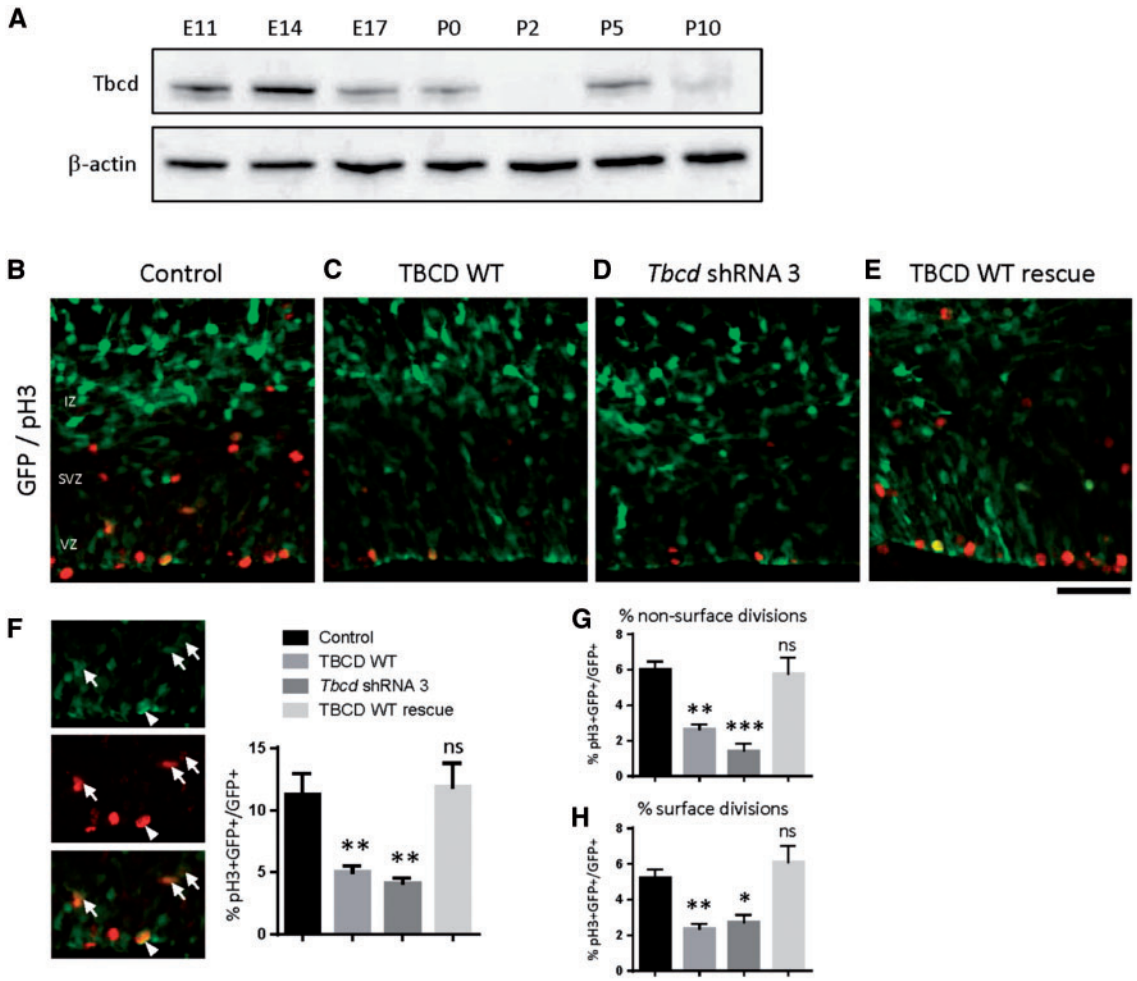

Figure 6. TBCD is detected in mouse brain lysates and perturbations in its expression impair cell proliferation. **(A)** Whole extracts of brain from mice at E11, E14, E17, P0, P2, P5 and P10 were analysed by Western blotting using a mouse-specific anti-tbcd antibody. A β-actin antibody was used as a loading control. Note the maximal expression at E14, with an additional burst at P5. **(B–E)** *In utero* electroporation of E14.5 cortical cells with the following combinations of shRNAs and expression constructs: non-targeting shRNA vector with empty mammalian expression vector (B), non-targeting shRNA vector with wild type *TBCD* (C), *tbcd*-targeting shRNA vector sh3 with empty mammalian expression vector (D), and *tbcd*-targeting shRNA vector sh3 with wild type *TBCD* expression vector (E). Successfully electroporated brain tissues were harvested 2 days later at E16.5 for cryosectioning and immunostaining. **(F)** Forced expression of wild type TBCD leads to a significant reduction in the expression of the mitotic marker pH3 (phosphorylated histone H3) when compared to treatment with a non-targeting (scr) shRNA vector control ($n = 4$–6 brains per condition). Similarly, treatment with sh3, a strong *tbcd* shRNA vecto, also leads to a significant reduction in pH3 co-expression. However, co-delivery of wild type TBCD can restore pH3 expression in sh3-treated cells to levels that are not significantly different to the control. **(G)** Quantification of pH3 + GFP+ indices away from the ventricular surface, defined as cells undergoing "non-surface" division and indicated by white arrows in (F). **(H)** Quantification of surface divisions, defined as pH3 + GFP+ indices immediately adjacent to the lateral ventricle, and indicated by an arrowhead in (F). Note that forced expression or knockdown of TBCD leads to a significant reduction in both non-surface (**G**: $F_{3,15} = 12$, $P = 0.0003$, one-way ANOVA, $n = 4$–6 per condition) and surface (**H**: $F_{3,15} = 19$, $P < 0.0001$, one-way ANOVA, $n = 4$–6 per condition) divisions, and that the knockdown phenotype is in either case restored to control levels upon co-delivery of wild type TBCD. Scale bar represents 50 micrometers; graphs represent mean ± SEM.

S7). These data suggest that forced expression or knockdown of tbcd affects neuroprogenitor proliferation in the developing mouse brain.

We next examined the effect of *tbcd* disruption on the radial migration of neurons, an important feature of their development within the embryonic cortex (25). The results of these experiments demonstrated that there is a significant interaction between treatment groups and the radial distribution of GFP-labelled cells within the E16.5 cortex (Fig. 7A–D and E; $F_{15,90} = 3.149$, $P = 0.0004$, Two-Way ANOVA, $n = 4$–6 brains per condition). Notably, we observed that overexpression of wild type TBCD (Fig. 7B) or sh3-mediated knockdown of endogenous *tbcd* (Fig. 7C) led to a significant reduction in the proportion of GFP-labelled cortical cells which migrated into the cortical plate (CP) (Fig. 7F, $F_{3,5} = 3.649$, $P = 0.0037$, one-way ANOVA). Intriguingly, we found that co-delivery of wild type TBCD restored the radial migration of cortical cells to levels that were not significantly different from the control condition (Fig. 7D). Thus, disruptions to *tbcd* influence the radial migration of embryonic cortical cells such that either too much or too little TBCD is detrimental to corticogenesis.

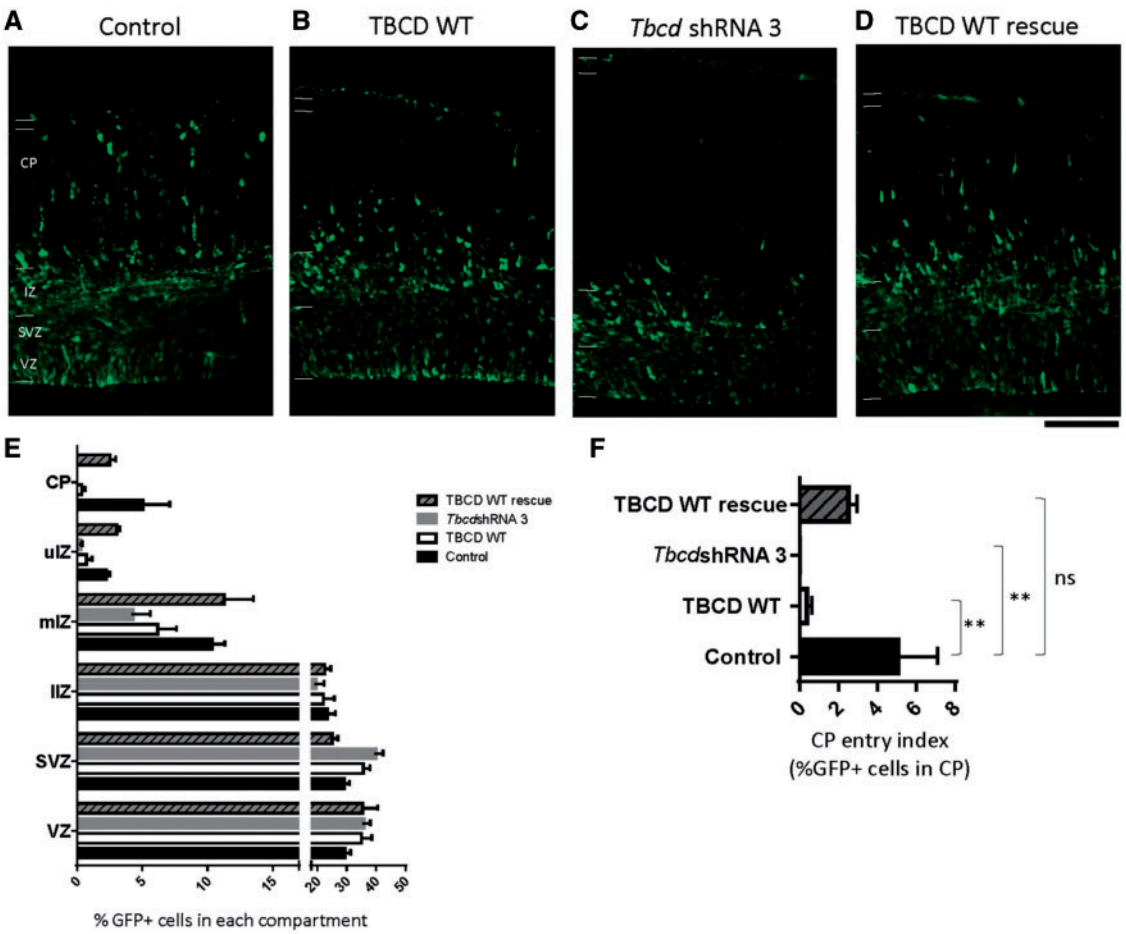

Figure 7. Induced changes in the level of tbcd lead to impaired radial migration within the embryonic E16.5 cortex. **(A–D)** *In utero* electroporation of E14.5 cortical cells with combinations of shRNAs and expression constructs and evaluated at E16.5. **(E)** There is a significant interaction between plasmid treatment and the distribution of GFP-labelled cells within cortical sub-compartments ($F_{15,90} = 3.149$, $P = 0.0004$, Two-WAY ANOVA, $n = 4$–6 per condition). **(F)** Analysis of the entry of cells into the Cortical Plate (CP) reveals a significant impairment upon forced expression of wild type TBCD or knockdown by shRNAs, but the defective migration of shRNA-treated cells is restored by co-delivery of wild type TBCD ($F_{3,5} = 3.649$, $P = 0.0037$, ** $P < 0.01$, one-way ANOVA, $n = 4$–6 per condition), indicative of defective migration. Scale bar represents 100 micrometers; graphs represent mean +/- SEM.

Mutant TBCDs in the context of neuroprogenitor proliferation and radial migration

We tested the ability of mutant (A475T and A586V) TBCDs to restore the shRNA3-induced reduction of pH3 expression in our electroporation studies. In these experiments, co-expression of shRNA3 with either wild type or mutant TBCDs resulted in an elevation of the number of GFP+ cells expressing pH3 to a level not statistically different from that detected in corresponding controls (Fig. 8A–F, $F_{4,19} = 5.293$, $P = 0.0049$, $n = 4$–6 per condition). The impairment in surface as well as non-surface division observed for pH3-expressing cells was also restored to levels not significantly different from the control (Fig. 8G and H). These data suggest an equivalent functional capacity of both mutant TBCD variants compared to wild type. Consistent with this inference, we found that the defective migration of *tbcd*-deficient cells following sh3 treatment could be restored by the A475T and A586V TBCD variants (Fig. 9). We did not observe a significant effect on cell death in these treatment groups, as measured by an examination of Casp3 expression (Supplementary Material, Fig. S7). Taken together, our *in utero* electroporation data reinforce the conclusions based on our biochemical and cell biological analyses, which demonstrate that the mutant TBCD proteins are functional, but are to some extent compromised compared to a wild type control.

Discussion

Here we describe four patients from two unrelated families each with distinct mutations in *TBCD*. *TBCD* is an essential gene initially characterized by virtue of the fact that the encoded protein was shown to be required for the de novo assembly of tubulin heterodimers (26). The patients would likely be classified as suffering from neurodegenerative disorders with brain atrophy and resultant secondary microcephaly. These are rare and catastrophic conditions that include a number of metabolic disorders and specific genetic aberrations affecting glial, neuronal or myelin maintenance and growth (3). Because TBCD is an indispensable component of the biochemical machinery required for tubulin heterodimer assembly, the diseases we describe here merit classification as a new kind of tubulinopathy. Among the tubulinopathies described to date, many of those involving mutation in tubulin-encoding genes (e.g. TUBA1A, TUBB2A, TUBB2B, TUBB2C and TUBB5) have been shown to be either

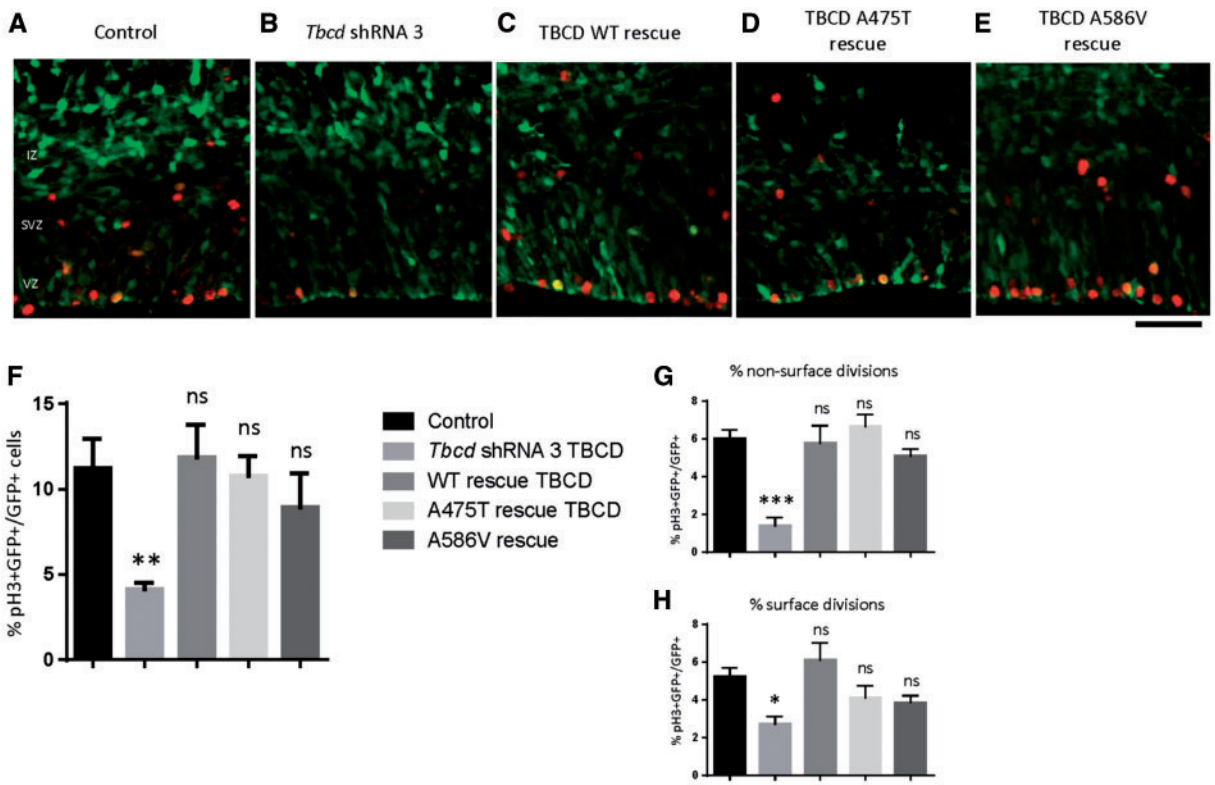

Figure 8. Tubulin and its disease-associated variants can restore pH3 expression in *tbcd* shRNA-treated cortical cells. **(A–E)** Effect of *in utero* electroporation performed on E14.5 mouse brains using combinations of shRNA vectors and TBCD expression constructs, as indicated. **(F)** There was a significant interaction between plasmid treatment and the expression of pH3 by GFP-labelled cells ($F_{4,19} = 5.293$, $P = 0.0049$, one-way ANOVA, $n = 4$–6 per condition). **(G, H)** Quantification of pH3 + GFP+ indices in cells distal to the ventricular surface **(G),** and in surface divisions **(H)** (see Legend to Fig. 5). Note that the significant reduction in non-surface divisions ($F_{4,19} = 16$, $P < 0.0001$, one-way ANOVA, $n = 4$–6 per condition) or surface divisions ($F_{4,19} = 5.4$, $P = 0.0046$, one-way ANOVA, $n = 4$–6 per condition) upon knockdown are restored to control levels upon co-delivery of either wild type TBCD, or the A475T or A586V variants. Scale bar represents 50 micrometers; graphs represent mean ± SEM.

causative of or associated with primary microcephaly. These tubulin isotypes are all abundantly expressed in the developing brain, either in post-mitotic neurons (TUBA1A, TUBB2B) or in post-mitotic neurons and radial glial or intermediate progenitors (TUBB5) (1,11). However, none of the hitherto described tubulinopathies have been associated with secondary microcephaly.

Both the *TBCD* mutations we describe result in a reduced intracellular level of the encoded protein in patient-derived skin fibroblasts, although in one case (A475T) the reduction is significantly greater than the other (A586V) (Fig. 3A). In neither case was there any evidence of a change in fibroblast microtubule architecture (Supplementary Material, Fig. S2). Neither mutation had any discernible effect on translational efficiency, folding or the integrity of the protein upon exposure to exogenous proteolysis ((43) Supplementary Material, Fig. S3). On the other hand, the A475T mutation resulted in a conspicuous reduction in *in vivo* half-life relative to a wild type control (Fig. 3B), and the intracellular level of TBCD in A475T patient-derived fibroblasts could be significantly increased by incubation of these cells in the presence of the proteasome inhibitor MG132 (Fig. 3C). We conclude that the reduced abundance of mutant proteins present in these patient cells is ascribable to proteolysis as a consequence of targeted destruction via the ubiquitin proteasome pathway. Their reduced intracellular abundance notwithstanding, our *in vitro* analyses showed that both mutant TBCD's were biochemically functional when assayed in either the forward (heterodimer assembly) or reverse (heterodimer disassembly) reactions (Supplementary Material, Fig. S1 and Fig 4A and B). The reverse reactions were particularly informative, because both mutant proteins showed a detectable quantitative functional impairment compared to the wild type control (Fig. 4B). This impaired biochemical activity was also evident in cultured cells: expression of the mutant TBCDs in HeLa cells in which the TBCD regulator Arl2 had been suppressed by treatment with siRNA (21) showed that the proportion of cells in which the microtubule network became decimated was substantially reduced compared to a wild type control (Fig. 5A and B). We infer from our biochemical and cell biological data that both mutations compromise, but do not abrogate the biological activity of the protein in terms of heterodimer assembly/disassembly.

In addition to their effect on heterodimer assembly and disassembly, it seems likely that other functions of TBCD may contribute to the pathophysiology of the diseases we describe, including an influence on various aspects of microtubule behaviour following neuroprogenitor proliferation and neuronal migration. For example, recent studies have reported such functions via analysis of a homozygous mutation in the *D. melanogaster* homolog of *TBCD*: when present in isolated projection neurons, this mutation resulted in microtubule disruption and ectopic arborization of neurites (27). Further analyses in *Drosophila* have established a physical interaction between TBCD and Dscam, a cell adhesion molecule that is important in neuronal development and that has been implicated in Down's syndrome. TBCD also interacts with Strip, a core component of the striatin-interacting phosphatase and kinase complex

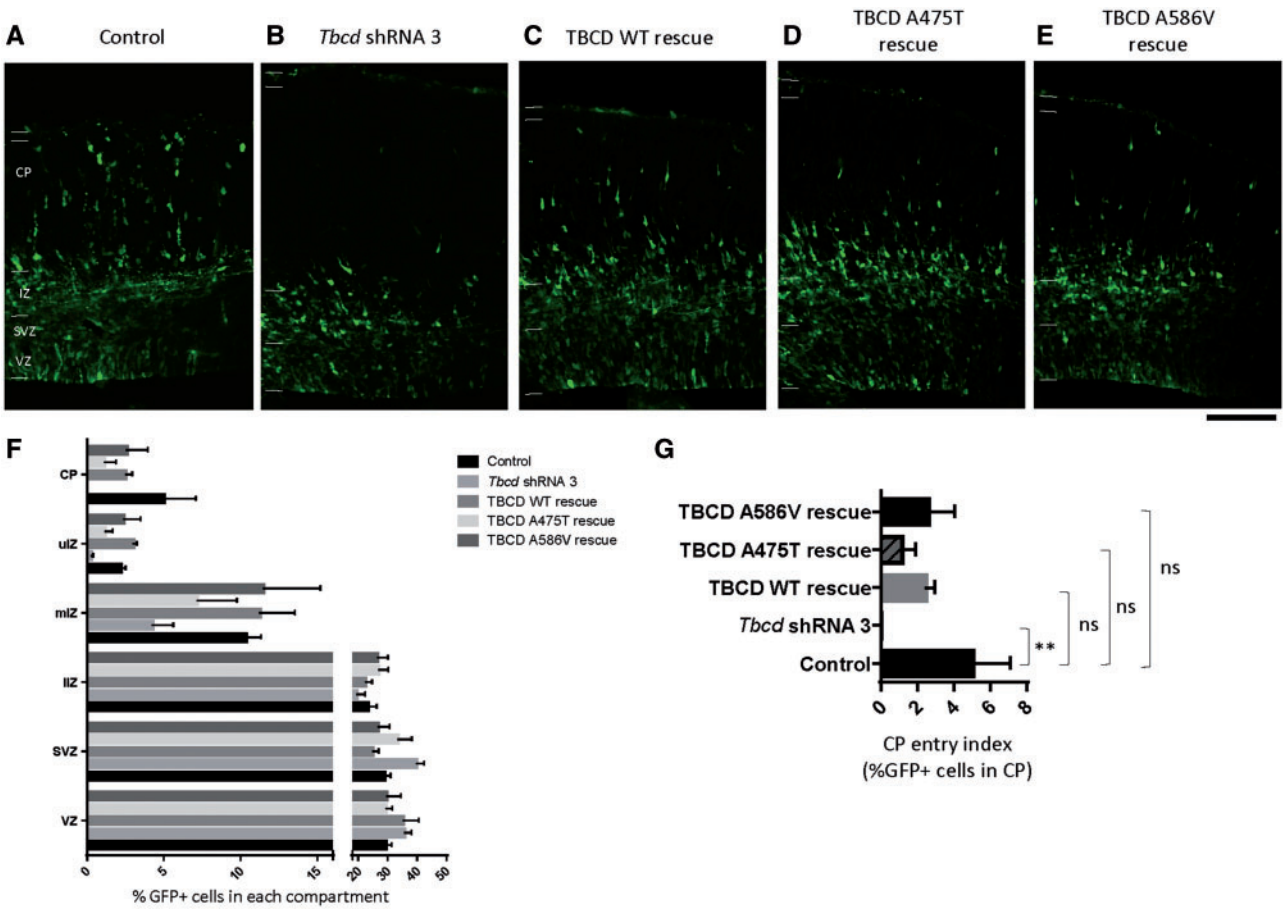

Figure 9. *TBCD* and its variants partially restore the defective radial migration of tbcd shRNA-treated cells. **(A–E)** Electroporation of combinations of shRNA vectors and TBCD expression constructs, as indicated. **(F)** A significant interaction exists between plasmid treatment and the radial distribution of GFP-labelled cells ($F_{20,114} = 2.571$, $P = 0.0009$, Two-WAY ANOVA, $n = 4$–6 animals per condition). **(G)** The defective migration of shRNA-treated cells could be restored by co-delivery of either wild type, A475T or A586V TBCD to levels not significantly different from the control ($F_{4,19} = 3.2$, $P = 3.293$, $P = 0.036$, one-way ANOVA, $n = 4$–6 animals per condition). Scale bar represents 100 micrometers; graphs represent mean ± SEM.

(STRIPAK) that is likely to influence microtubule stability. Strip also genetically interacts with Dscam (27). We note that the mutated human TBCD residues reported here (A475 and A586) are conserved in the *D. melanogaster* homolog (data not shown). There is also evidence that TBCD is concentrated at the centrosome and midbody in a cell cycle dependent manner, and that it participates in centriologenesis, spindle organization and cell abscission (28). Taken together, these observations point to multiple interactions of TBCD with effectors that modulate microtubule behaviour during neuronal morphogenesis. Indeed, such interactions could well be compromised by the mutations we describe: although no structural information is currently available for TBCD, a theoretical domain analysis of the encoded sequence reveals the presence of HEAT (ARM-like) repeats characterized by the presence of pairs of antiparallel helices stacked in a consecutive array (29). Such motifs are thought to be involved in protein-protein interactions (30).

We extended our biochemical analyses by examining the effect of perturbing TBCD abundance in the context of the developing intact mammalian brain, and found that shRNA-induced suppression of TBCD expression in embryonic cortical cells of E14.5 mice resulted in a conspicuous reduction in cell proliferation as measured by the abundance of pH3-positive cells (Fig. 6). Significantly, the suppression of both surface and non-surface divisions suggests a pleiotropic effect of TBCD disruption on the proliferative capacity of neuroprogenitor subtypes, including both radialglial cells (RGCs) which undergo self-renewing divisions and intermediate progenitor cells (IPCs) which typically undergo terminal neurogenic divisions (31). Given that TBCD is essential for life (32–34) and that tubulin and microtubules are indispensable components for cell division, a deficiency in TBCD activity would be expected to have deleterious developmental consequences, particularly in a context where there is an exceptionally high requirement for de novo heterodimer assembly. Equally, the fact that the heterodimer assembly reaction is readily reversible and that an excess of TBCD can disrupt the tubulin heterodimer *in vitro* and *in vivo* (Figs. 4B and 5) is consistent with our finding that overexpression of wild type TBCD in the developing mouse cortex also induces a reduction in neuroprogenitor proliferation (Fig. 6). Our finding that the TBCD mutations we describe yield proteins that are somewhat functionally compromised is also consistent with our *in utero* electroporation experiments in which expression of either TBCD mutant protein was found to restore pH3 expression in tbcd shRNA-treated cortical cells (Fig. 6).

Our data showed that the biochemical and cell biological deficiencies associated with *TBCD* A475T are greater than those associated with *TBCD* A586V in terms of heterodimer assembly/

disassembly. This was reflected in the reduced relative ability of TBCD A475T to function in the back-reaction (Fig. 4B) and to destroy the microtubule network upon overexpression *in vivo* (Fig. 5A and B). On the other hand, the clinical features associated with each mutation are quite similar (Table 1). This fact could reflect different effects of each mutation in terms of interaction of TBCD with known effectors such as Arl2 (20,35), PP2A (36) and Dscam (27). Additionally, we cannot exclude the existence of other genetic traits in the patients we describe that might contribute to the phenotype. The latter inference is consistent with a recent report suggesting that a mutation in *TBCD* can contribute to a cortical malformation in the context of mutation in *WDR62* (37). Given the especially high demand for tubulin during corticogenesis and neuronal migration (10,24) and our demonstration of a concurrent requirement for an adequate supply of TBCD (Fig. 6), it seems likely that a significant contributing factor to the pathogenesis of the diseases we describe is a limitation in de novo neuronal tubulin production caused by a paucity of functional TBCD, and that functional deficiency incurred by mutation in *TBCD* can contribute to microcephaly. Equally, the defective migration of neurons following TBCD perturbation implies a coordinated involvement of the microtubule cytoskeleton in both neurite outgrowth and directional movement (24,38). We note that mutations in *TBCE*, which encodes a protein that interacts directly with TBCD in the de novo assembly of the tubulin heterodimer, have also been shown to cause severe cortical (and other) developmental defects as part of the syndrome known as HRD (hypoparathyroidism, mental retardation and dysmorphism) (18,39). The construction and analysis of mouse models that accurately mimic the TBCD mutations we describe is likely to prove a useful adjunct to the data reported here.

Materials and Methods

Whole exome analysis

Exonic sequences were enriched in the DNA sample of patients AII-1 and BII-1 using the SureSelect Human All Exon 50 Mb Kit (Agilent Technologies, Santa Clara, California, USA). Sequences were determined by HiSeq2000 (Illumina, San Diego, California, USA) as 100-bp paired-end runs. Data analysis including read alignment and variant calling was performed using DNAnexus software (Palo Alto, California, USA) using the default parameters with the human genome assembly hg19 (GRCh37) as reference. Parental consent was given for DNA studies. The study was performed with the approval of the ethical committees of Hadassah Medical Center and the Ministry of Health.

Skin fibroblasts and western blotting

Age-matched wild type or patient skin fibroblasts were grown in F10 medium supplemented with 20% foetal calf serum. Whole cytoplasmic extracts were prepared by washing the cells in PBS followed by suspension in 0.2 ml ice-cold buffer (10 mM Tris-HCl pH 7.4, 1 mM $MgCl_2$, 1 mM EGTA plus a protease inhibitor cocktail [Roche Life Sciences, Inc.]) in 2 ml Eppendorf centrifuge tubes. The cells were lysed with an electrically driven micro-Dounce homogenizer and the homogenate centrifuged for 10 min at 15,000*g*. The protein content of the supernatants was determined using the Biorad Protein reagent; aliquots were stored at -70°C following flash freezing in liquid N_2. Samples containing 10 μg of protein were resolved by 8% SDS-PAGE, transferred to nitrocellulose and probed with a rabbit antibody to human TBCD (21), a monoclonal anti-α-tubulin antibody, or a monoclonal anti-β-actin antibody used as a loading control.

Plasmid constructs, transfection and immunofluorescence

Plasmid constructs encoding either a full-length human wild type or mutant TBCD cDNA were assembled in the pcDNA3 vector (Invitrogen, Inc.), checked by DNA sequencing and transfected into HEK 293 cells contained in individual 60mM culture dishes and grown in DMEM supplemented with 10% foetal calf serum. Transfection was done using the Fugene transfection reagent (Roche Life Sciences, Inc.). In experiments to determine the effect of TBCD expression on microtubule architecture, HeLa cells grown in DMEM supplemented with 10% fetal calf serum were transfected with siRNAs targeting the expression of Arl2 as previously described (21), followed by transfection with plasmid constructs engineered for the expression of either wild type or mutant-bearing sequences encoding TBCD. 48 h post-transfection, cells were fixed with paraformaldehyde and examined by immunofluorescence with an anti-human TBCD antibody and an anti-α-tubulin antibody as described (21).

Determination of TBCD half-life and measurement of intracellular TBCD abundance following proteasome inhibition

Plasmid constructs encoding either a full-length human wild type or mutant TBCD cDNA were assembled in the pcDNA3 vector (Invitrogen, Inc.), checked by DNA sequencing and transfected into HEK293 cells contained in individual 60mM culture dishes and grown in DMEM supplemented with 10% foetal calf serum. Transfection was done using the Fugene 6 transfection reagent (Roche Life Sciences, Inc.). 42 h post-transfection, cycloheximide (CHX; final concentration, 0.7 mM) was added to the cultures. At various intervals thereafter (see Supplementary Material, Fig. S4), cytosolic extracts were prepared as follows: cells were washed with PBS and suspended by scraping into ice-cold buffer (0.2 ml) containing 10 mM Tris-HCl, pH 7.2, 10 mM NaCl, 0.5% NP40 and a cocktail of protease inhibitors (Roche, Life Sciences, Inc.). The suspension was centrifuged at 15,000 x g and the TBCD content of the supernatants determined by Western blotting of aliquots containing equal amounts (10 μg) of total protein using a specific anti-human TBCD antibody (21). An anti-Cullin-1 antibody was used as a loading control. In experiments to determine the effect on TBCD levels of incubation in the presence of a proteasome inhibitor, primary wild type or A475T patient-derived fibroblasts were incubated for 12 h in the presence of 12 μM MG132; extracts were prepared and analysed as described above. An anti β-actin antibody was used as a loading control.

Transcription/translation reactions and analysis of reaction products

Coupled transcription/translation reactions were done in rabbit reticulocyte lysate (Quick-coupled TNT, Promega Inc.) supplemented with ^{35}S-methionine (0.1 mCi/ml; specific activity 1000 Ci/mMole; Perkin-Elmer, Inc.). In experiments to determine the relative functional efficacy of mutant forms of TBCD (see text and Fig. 2B), with the exception of a control reaction (done

to reveal the migration position of endogenous reaction products of rabbit origin), the reactions were incubated at 30°C for 30 min before supplementation with either recombinant human wild type or mutant TBCD (0.15μg/ml final concentration) (18). The incubations were then continued for a further 30 min. The reaction products were divided equally; one aliquot was supplemented with native tubulin heterodimers (18) to a concentration of 1.0 mg/ml so as to chase the TBCD/β-tubulin intermediates into de novo assembled heterodimers, and each reaction was incubated for a further 30 min. Reaction products were resolved on 4.5% native polyacrylamide gels as described previously (10,42) and detected by autoradiography.

Tubulin heterodimer disruption reactions and preparation of recombinant TBCDs

Tubulin heterodimers labelled in their β-subunits were generated by expression in rabbit reticulocyte lysate and purified by anion exchange chromatography as described previously (21). Aliquots containing equal amounts of labelled heterodimers were incubated with various stoichiometric ratios (1x, 2x or 4x) of the recombinant wild type or mutant TBCD prepared as follows. HEK293S GnTI cells grown in suspension were transfected using polyethylenimine (40) with constructs engineered for the expression of N-terminally His_6-tagged human wild type and mutant TBCDs contained in the pcDNA 3+ vector. Previous studies have shown that placement of an N-terminal tag on TBCD has no detectable impact on the biological activity of TBCD *in vivo* (20). 44 h post transfection, cells were harvested, washed twice with cold PBS, lysed by homogenization in ice-cold buffer (10 mM $NaP0_4$ buffer, pH 7.0, 1 mM each of EGTA, $MgCl_2$ and protease inhibitors) using a glass Dounce homogenizer, and the homogenate cleared of particulate material by two successive centrifugation steps at 10,000 and 200,000*g*. The resulting supernatant was adjusted to 0.3 M NaCl and to 50 mM $NaPO_4$ buffer, pH 7.0, and passed over a 0.8 x 1.0 cm column of Talon Superflow metal affinity resin (Clontech, Inc.) following the manufacturer's recommendations. After extensive washing, the columns were eluted with affinity column buffer containing 0.15 M imidazole, pH 7.0. The recovered proteins were concentrated using a Millipore Centricon 30 device and their content of recombinant protein determined by Western blotting with an antibody that specifically detects human TBCD (21).

In utero electroporation

All procedures were performed in accordance with guidelines set out by the Perkins Animal Ethics Committee at the University of Western Australia (AEC021), and in accordance with guidelines set out by the National Health and Medical Research Council of Australia. *In utero* electroporation was performed on E14.5 embryos of time-mated C57/Black6J mice as previously indicated (10), with the following modifications. Inhalable anaesthesia (isofluorane) was utilized in conjunction with a suitable analgesic (buprenorphine) at prescribed times throughout the surgical procedure on the pregnant dam. Four hairpin sequences which target *tbcd* (5' TTCCTCACGAAGTGG CTAATGTTCAGCCT 3'; 5' TTATTGCTGGCTTCCAGGAATACACC AAG 3', 5' CAGGCTTGTCACAGACTATCTGGATGAGA 3', 5' TCCA GTTGTAAGAGAACAGCGGAATCGCC 3') were cloned into the ApaI and EcoRV sites of our shRNA vector (41). Full details are available upon request. DNA injections were carried out with 1μg/μl of each constituent plasmid (pSil-Caggs shRNA vector and mammalian expression vector pCDNA3). Successfully electroporated animals were verified by GFP epifluorescence inspection. Brains were dissected and preserved in fixative (4% paraformaldehyde/phosphate-buffered saline) overnight before processing for cryostat sectioning and immunostaining as previously indicated (10). Immunostaining was performed with the following primary antibodies: chicken anti-GFP (Ab13970, Abcam), rabbit anti-phosphorylated Histone-H3(ser10) (06-570, Merck Millipore, 1:1000), anti-activated Caspase-3 (R&D Systems) together with appropriate secondary antibodies conjugated with fluorophores (Molecular Probes). Cell nuclei were visualized with DAPI (4'6-Diamidino-2-Phenylindole). Images of brain sections were captured on an epifluorescence microscope (BX51, Olympus) equipped with a CCD camera (Nikon, Japan). Subdivisions of the embryonic cortex (VZ/SVZ, IZ and CP) were identified based on cell density as visualised with DAPI staining. Cell counting was performed blind to the condition on representative fields of sections of electroporated brains using ImageJ software.

Supplementary Material

Supplementary Material is available at *HMG* online.

Conflict of Interest statement. None declared.

Funding

N.J.C. acknowledges the receipt of a grant (R01GM097376) from the National Institutes of Health. J. I-T. H. is a recipient of an NHMRC Career Development Award (ID:1011505) from the Health and Medical Research Council of Australia.

References

1. Gilmore, E.C. and Walsh, C.A. (2013) Genetic causes of microcephaly and lessons for neuronal development. *Wiley Interdiscip. Rev. Dev. Biol.*, **2**, 461–478.
2. Stiles, J. and Jernigan, T.L. (2010) The basics of brain development. *Neuropsychol. Rev.*, **20**, 327–348.
3. Seltzer, L.E. and Paciorkowski, A.R. (2014) Genetic disorders associated with postnatal microcephaly. *Am. J. Med. Genet. C Semin. Med. Genet.*, **166C**, 140–155.
4. Keays, D.A., Tian, G., Poirier, K., Huang, G.J., Siebold, C., Cleak, J., Oliver, P.L., Fray, M., Harvey, R.J., Molnar, Z., *et al.* (2007) Mutations in alpha-tubulin cause abnormal neuronal migration in mice and lissencephaly in humans. *Cell*, **128**, 45–57.
5. Tian, G., Jaglin, X.H., Keays, D.A., Francis, F., Chelly, J. and Cowan, N.J. Disease-associated mutations in TUBA1A result in a spectrum of defects in the tubulin folding and heterodimer assembly pathway. *Hum. Mol. Genet.*, **19**, 3599–3613.
6. Jaglin, X.H. and Chelly, J. (2009) Tubulin-related cortical dysgeneses: microtubule dysfunction underlying neuronal migration defects. *Trends Genet.*, **25**, 555–566.
7. Cushion, T.D., Dobyns, W.B., Mullins, J.G., Stoodley, N., Chung, S.K., Fry, A.E., Hehr, U., Gunny, R., Aylsworth, A.S., Prabhakar, P., *et al.* (2013) Overlapping cortical malformations and mutations in TUBB2B and TUBA1A. *Brain*, **136**, 536–548.
8. Tischfield, M.A., Baris, H.N., Wu, C., Rudolph, G., Van Maldergem, L., He, W., Chan, W.M., Andrews, C., Demer, J.L., Robertson, R.L., *et al.* Human TUBB3 mutations perturb

microtubule dynamics, kinesin interactions, and axon guidance. *Cell*, **140**, 74–87.
9. Poirier, K., Saillour, Y., Bahi-Buisson, N., Jaglin, X.H., Fallet-Bianco, C., Nabbout, R., Castelnau-Ptakhine, L., Roubertie, A., Attie-Bitach, T., Desguerre, I., *et al.* (2010) Mutations in the neuronal ss-tubulin subunit TUBB3 result in malformation of cortical development and neuronal migration defects. *Hum. Mol. Genet.*, **19**, 4462–4473.
10. Breuss, M., Heng, J.I., Poirier, K., Tian, G., Jaglin, X.H., Qu, Z., Braun, A., Gstrein, T., Ngo, L., Haas, M., *et al.* (2012) Mutations in the beta-tubulin gene TUBB5 cause microcephaly with structural brain abnormalities. *Cell Rep.*, **2**, 1554–1562.
11. Breuss, M. and Keays, D.A. (2014) Microtubules and neurodevelopmental disease: the movers and the makers. *Adv. Exp. Med. Biol.*, **800**, 75–96.
12. Cowan, N.J.a.L., S.A. (2002) Type II chaperonins, prefoldin and the tubulin-specific chaperones. *Advances in Prot. Chem.*, **59**, 73–104.
13. Vainberg, I.E., Lewis, S.A., Rommelaere, H., Ampe, C., Vandekerckhove, J., Klein, H.L. and Cowan, N.J. (1998) Prefoldin, a chaperone that delivers unfolded proteins to cytosolic chaperonin. *Cell*, **93**, 863–873.
14. Leitner, A., Joachimiak, L.A., Bracher, A., Monkemeyer, L., Walzthoeni, T., Chen, B., Pechmann, S., Holmes, S., Cong, Y., Ma, B., *et al.* (2012) The molecular architecture of the eukaryotic chaperonin TRiC/CCT. *Structure*, **20**, 814–825.
15. Tian, G., Vainberg, I.E., Tap, W.D., Lewis, S.A. and Cowan, N.J. (1995) Quasi-native chaperonin-bound intermediates in facilitated protein folding. *J. Biol. Chem.*, **270**, 23910–23913.
16. Poirier, K., Lebrun, N., Broix, L., Tian, G., Saillour, Y., Boscheron, C., Parrini, E., Valence, S., Pierre, B.S., Oger, M., *et al.* (2013) Mutations in TUBG1, DYNC1H1, KIF5C and KIF2A cause malformations of cortical development and microcephaly. *Nat. Genet.*, **45**, 639–647.
17. Wang, D., Villasante, A., Lewis, S.A. and Cowan, N.J. (1986) The mammalian beta-tubulin repertoire: hematopoietic expression of a novel, heterologous beta-tubulin isotype. *J. Cell Biol.*, **103**, 1903–1910.
18. Tian, G., Huang, M.C., Parvari, R., Diaz, G.A. and Cowan, N.J. (2006) Cryptic out-of-frame translational initiation of TBCE rescues tubulin formation in compound heterozygous HRD. *Proc. Natl Acad. Sci. U S A*, **103**, 13491–13496.
19. Tian, G., Lewis, S.A., Feierbach, B., Stearns, T., Rommelaere, H., Ampe, C. and Cowan, N.J. (1997) Tubulin subunits exist in an activated conformational state generated and maintained by protein cofactors. *J. Cell Biol.*, **138**, 821–832.
20. Bhamidipati, A., Lewis, S.A. and Cowan, N.J. (2000) ADP ribosylation factor-like protein 2 (Arl2) regulates the interaction of tubulin-folding cofactor D with native tubulin. *J. Cell Biol.*, **149**, 1087–1096.
21. Tian, G., Thomas, S. and Cowan, N.J. Effect of TBCD and its regulatory interactor Arl2 on tubulin and microtubule integrity. *Cytoskeleton (Hoboken)*, **67**, 706–714.
22. Takahashi, T., Nowakowski, R.S. and Caviness, V.S. Jr. (1996) The leaving or Q fraction of the murine cerebral proliferative epithelium: a general model of neocortical neuronogenesis. *J. Neurosci.*, **16**, 6183–6196.
23. Takahashi, T., Nowakowski, R.S. and Caviness, V.S. Jr. (1996) Interkinetic and migratory behavior of a cohort of neocortical neurons arising in the early embryonic murine cerebral wall. *J. Neurosci.*, **16**, 5762–5776.
24. Ngo, L., Haas, M., Qu, Z., Li, S.S., Zenker, J., Teng, K.S., Gunnersen, J.M., Breuss, M., Habgood, M., Keays, D.A., *et al.* (2014) TUBB5 and its disease-associated mutations influence the terminal differentiation and dendritic spine densities of cerebral cortical neurons. *Hum. Mol. Genet.*, **23**, 5147–5158.
25. Greig, L.C., Woodworth, M.B., Galazo, M.J., Padmanabhan, H. and Macklis, J.D. (2013) Molecular logic of neocortical projection neuron specification, development and diversity. *Nat. Rev. Neurosci.*, **14**, 755–769.
26. Tian, G., Huang, Y., Rommelaere, H., Vandekerckhove, J., Ampe, C. and Cowan, N.J. (1996) Pathway leading to correctly folded beta-tubulin. *Cell*, **86**, 287–296.
27. Okumura, M., Sakuma, C., Miura, M. and Chihara, T. (2015) Linking cell surface receptors to microtubules: tubulin folding cofactor D mediates Dscam functions during neuronal morphogenesis. *J. Neurosci.*, **35**, 1979–1990.
28. Fanarraga, M.L., Bellido, J., Jaen, C., Villegas, J.C. and Zabala, J.C. TBCD links centriologenesis, spindle microtubule dynamics, and midbody abscission in human cells. *PLoS One*, **5**, e8846.
29. Grynberg, M., Jaroszewski, L. and Godzik, A. (2003) Domain analysis of the tubulin cofactor system: a model for tubulin folding and dimerization. *BMC Bioinformatics*, **4**, 46.
30. Groves, M.R., Hanlon, N., Turowski, P., Hemmings, B.A. and Barford, D. (1999) The structure of the protein phosphatase 2A PR65/A subunit reveals the conformation of its 15 tandemly repeated HEAT motifs. *Cell*, **96**, 99–110.
31. Florio, M. and Huttner, W.B. (2014) Neural progenitors, neurogenesis and the evolution of the neocortex. *Development*, **141**, 2182–2194.
32. Hirata, D., Masuda, H., Eddison, M. and Toda, T. (1998) Essential role of tubulin-folding cofactor D in microtubule assembly and its association with microtubules in fission yeast. *Embo J.*, **17**, 658–666.
33. Radcliffe, P.A., Hirata, D., Vardy, L. and Toda, T. (1999) Functional dissection and heirarchy of tubulin-folding cofactors in fission yeast. *Mol. Biol. Cell*, **10**, 2987–3001.
34. Steinborn, K., Maulbetsch, C., Priester, B., Trautmann, S., Pacher, T., Geiges, B., Kuttner, F., Lepiniec, L., Stierhof, Y.D., Schwarz, H., *et al.* (2002) The Arabidopsis PILZ group genes encode tubulin-folding cofactor orthologs required for cell division but not cell growth. *Genes Dev.*, **16**, 959–971.
35. Chen, K., Koe, C.T., Xing, Z.B., Tian, X., Rossi, F., Wang, C., Tang, Q., Zong, W., Hong, W.J., Taneja, R., *et al.* (2016) Arl2- and Msps-dependent microtubule growth governs asymmetric division. *J. Cell Biol.*, **212**, 661–676.
36. Shern, J.F., Sharer, J.D., Pallas, D.C., Bartolini, F., Cowan, N.J., Reed, M.S., Pohl, J. and Kahn, R.A. (2003) Cytosolic Arl2 is complexed with cofactor D and protein phosphatase 2A. *J. Biol. Chem.*, **278**, 40829–40836.
37. Poulton, C.J., Schot, R., Seufert, K., Lequin, M.H., Accogli, A., Annunzio, G.D., Villard, L., Philip, N., de Coo, R., Catsman-Berrevoets, C., *et al.* (2014) Severe presentation of WDR62 mutation: is there a role for modifying genetic factors?. *Am. J. Med. Genet. Part a*, **164A**, 2161–2171.
38. Smith, A.B., 3rd, Charnley, A.K., Mesaros, E.F., Kikuchi, O., Wang, W., Benowitz, A., Chu, C.L., Feng, J.J., Chen, K.H., Lin, A., *et al.* (2005) Design, synthesis, and binding affinities of pyrrolinone-based somatostatin mimetics. *Org. Lett.*, **7**, 399–402.
39. Parvari, R., Hershkovitz, E., Grossman, N., Gorodischer, R., Loeys, B., Zecic, A., Mortier, G., Gregory, S., Sharony, R., Kambouris, M., *et al.* (2002) Mutation of TBCE causes hypoparathyroidism-retardation-dysmorphism and autosomal recessive Kenny-Caffey syndrome. *Nat. Genet.*, **32**, 448–452.
40. Longo, P.A., Kavran, J.M., Kim, M.S. and Leahy, D.J. (2013) Transient mammalian cell transfection with polyethylenimine (PEI). *Methods Enzymol.*, **529**, 227–240.

41. Bron, R., Vermeren, M., Kokot, N., Andrews, W., Little, G.E., Mitchell, K.J. and Cohen, J. (2007) Boundary cap cells constrain spinal motor neuron somal migration at motor exit points by a semaphorin-plexin mechanism. *Neural Dev.*, **2**, 21.
42. Jaglin, X.H., Poirier, K., Saillour, Y., Buhler, E., Tian, G., Bahi-Buisson, N., Fallet-Bianco, C., Phan-Dinh-Tuy, F., Kong, X.P., Bomont, P., *et al.* (2009) Mutations in the beta-tubulin gene TUBB2B result in asymmetrical polymicrogyria. *Nat. Genet.*, **41**:746–752.
43. Tian, G., Vainberg, I.E., Tap, W.D., Lewis, S.A. and Cowan, N.J. (1995) Specificity in chaperonin-mediated protein folding. *Nature*, **375**, 250–253.